Organic & Biomolecular Chemistry

ROYAL SOCIETY OF CHEMISTRY

PAPER

View Article Online
View Journal

Cite this: DOI: 10.1039/d6ob00581k

Linker dependence of $^1O_2$ generation by G4-binding tetra-imidazolium porphyrins

Çetin Çelik, [a] Naoko Kakusho, [b] Tianyu Xu, [a] Sung Sik Lee, [c] Naoko Yoshizawa-Sugata, *[d] Hisao Masai *[b] and Yoko Yamakoshi *[a]

Received 9th April 2026,
Accepted 12th May 2026

DOI: 10.1039/d6ob00581k

rsc.li/obc

Three water-soluble porphyrins with tetracationic imidazolium groups were synthesized and assessed for complexation with human telomeric guanine-quadruplex (G4) DNA. Based on UV-vis titration studies, these porphyrins showed 10-fold higher complexation stability toward G4 DNA over non-G4 DNA. This was consistent with FRET experimental data, which showed that G4 stabilization by these porphyrins was significantly enhanced in comparison with that of non-G4 DNA. The porphyrins had slightly longer absorption wavelengths than a previously reported cationic porphyrin with the same functional groups but shorter linkers, indicating that they may be more suitable as photosensitizers (PSs) for photodynamic therapy (PDT). Significant photoinduced singlet oxygen ($^1O_2$) generation of these porphyrins was observed by the ESR spin-trapping method under irradiation with deep red LED light (max at 660 nm). In the presence of telo24 G4 DNA, this photoinduced $^1O_2$ generation was enhanced. Cellular internalization of these porphyrins was observed by flow cytometry, resulting in sufficient photocytotoxicity of these porphyrins toward both cancer cells (HeLa) and normal cells (NHDF). Photocytotoxicity to a cancer cell line was higher than that to normal cells. Although this mechanism was not clearly explained, the results show superior properties of these porphyrin molecules reported here as PDT-PSs.

Introduction

Cationic porphyrins, including TMPyP4, are often known as ligands for guanine-quadruplex (G4) DNAs.[1–4] G4s are some of the non-B secondary structures of DNA or RNA and observed in guanine (G)-rich sequences. In the presence of cations (*e.g.* K^+ and Na^+), four G bases form a tetrad structure *via* Hoogsteen-type hydrogen bonding and stack with each other to form G4. Recently, G4s have been identified as potential therapeutic targets for various diseases, including cancers.[5,6] For instance, promoter regions of many oncogenes, *e.g. MYC*, *VEGF*, *KRAS*, and *BCL2*, often contain G-rich sequences, which potentially form G4 structures. By stabilizing these G4s with specific ligands, the corresponding oncogenes can be downregulated.[7–9] Alternatively, G4 binders often inhibit telomerase, which plays an important role in the elongation of telomere repeats (TTAGGG).[10,11] These telomere repeats are essential for the proliferation of cancer cells, resulting in the specific effects of G4-binders on cancer cells over normal cells. A number of G4 binders including porphyrin derivatives have been reported.

In addition to their G4-binding properties, porphyrins are known as efficient photosensitizers (PSs) for photodynamic therapy (PDT). PDT is a non-surgical treatment for various diseases including cancers, and the majority of FDA-approved PDT-PSs are porphyrin derivatives. It involves PS molecules, visible light – ideally in the therapeutic window (650–800 nm)[12] – and molecular oxygen ($^3O_2$). Under visible light irradiation, porphyrins trigger the conversion of $^3O_2$ to singlet oxygen ($^1O_2$), a reactive oxygen species (ROS) that damages the tissues nearby.[13,14] Recently, G4-targeting PSs have attracted attention for the selective treatment of cancer cells[15–22] due to their increased abundance of G4 DNA.[23–25] In addition, G is prone to oxidation, forming 8-oxo-guanine, because of its lowest oxidation potential among all DNA/RNA bases.[26] Taken together, combined with porphyrins' tendency to localize in cancer cells,[27] the ability to use G4-binding porphyrins as a PS offers potential for selective treatment of cancer cells. Towards this aim, TMPyP4, a well-studied G4-binding porphyrin with photoinduced $^1O_2$ generation, was investigated for this application, but it showed relatively low selectivity in binding to G4 over non-G4 DNA and low cellular uptake.[28]

[a]*Department of Chemistry and Applied Biosciences, ETH Zürich, Vladimir-Prelog-Weg 3, CH-8093 Zürich, Switzerland. E-mail: yamakoshi@org.chem.ethz.ch*
[b]*Department of Basic Medical Sciences, Tokyo Metropolitan Institute of Medical Science, 2-1-6 Kamikitazawa, Setagaya, Tokyo 156-8506, Japan. E-mail: masai-hs@igakuken.or.jp*
[c]*ScopeM, ETH Zürich, Otto-Stern-Weg 3, CH-8093 Zürich, Switzerland*
[d]*Research Center for Genome & Medical Sciences, Tokyo Metropolitan Institute of Medical Science, 2-1-6 Kamikitazawa, Setagaya, Tokyo 156-8506, Japan. E-mail: yoshizawa-nk@igakuken.or.jp*

Recently, we have reported two tetracationic porphyrins, with tetra-guanidinium and tetra-imidazolium moieties.[26] These water-soluble porphyrins revealed both G4 binding and photoinduced $^1O_2$ generation properties. In several *in vitro* tests, the porphyrin with tetra-imidazolium cations presented superior properties with higher binding stability toward G4 DNA and better cellular internalization in comparison with TMPyP4, resulting in enhanced photocytotoxicity to a cancer cell line over normal cells. In this study, we synthesized the tetra-imidazolium cationic porphyrins with longer linkers. We postulated that these tetracationic porphyrins **1–3** (Fig. 1) may show improved G4-binding and photosensitization properties due to their longer linkers. The synthesized porphyrins **1–3** were characterized in detail with respect to their G4 stabilizing ability, photoinduced $^1O_2$ generation, photoinduced DNA damage, internalization into cells, and photocytotoxicity, in comparison with our previously reported porphyrin **4**.

Results and discussion

Syntheses of porphyrins 1, 2, and 3

Porphyrins **1**, **2**, and **3** were synthesized by a standard method, as shown in Scheme S1 in the SI. The porphyrins **S4–6** were prepared from aldehydes **S1–3** and pyrrole *via* the Lindsey method and converted to porphyrins **1–3** by a nucleophilic addition of 1-methyl imidazole. The resulting porphyrins were purified by reverse-phase HPLC and treated with Dowex for anion exchange to provide Cl^- salts exhibiting a single peak in HPLC (Fig. S17, S25 and S33). Porphyrins **1**, **2**, and **3** were characterized by ^1H, ^{13}C NMR, HRMS, and FT-IR-ATR to clearly confirm their structures (data are given in the SI). In HRMS measurements, molecular ion peaks corresponding to the *m*/*z* of M^{4+}, $[M - H]^{3+}$, and $[M + H]^{5+}$ were observed for all three porphyrins (Fig. S15, S23, and S31). UV-vis spectra revealed one Soret band and four Q-bands, in line with the typical characteristics of metal-free porphyrins (Fig. 2a). Both the Soret band and the Q-bands of porphyrins **1–3** were red-shifted in comparison with those of our previous imidazole porphyrin **4**,[29] presumably due to the O-atoms being connected to aromatic rings. In particular, the longest Q-band observed for each porphyrin **1–3** was at a maximum of *ca.* 654 nm, significantly shifted to a longer wavelength in comparison with that for **4**, which has a maximum at *ca.* 640 nm (Fig. S42). This red shift in the excitation wavelength of PS is advantageous for PDT, which requires a light source with longer wavelengths due to their better tissue penetration. A slight increase in absorption intensity of the longest Q-band was observed upon the increase of linker length (**1** < **2** < **3**). All porphyrins were fluorescent, as shown in Fig. 2b.

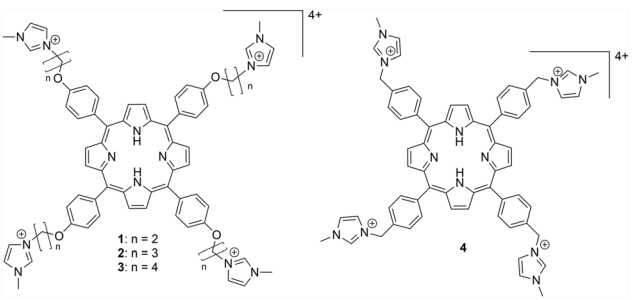

Fig. 1 Chemical structures of tetracationic porphyrins **1–3** developed in this study and previously reported porphyrin **4**.

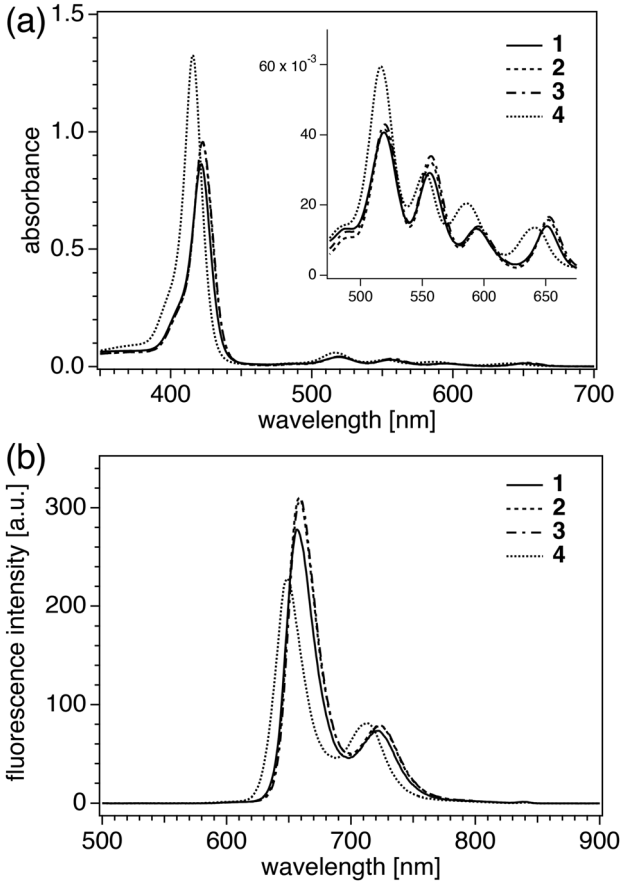

Fig. 2 (a) UV-vis spectra of porphyrins **1–4**. (b) Fluorescence spectra of porphyrins **1–4** using an excitation wavelength of 423 nm and a slit width of 5 nm. All measurements were conducted with 5 μM solution in pH 7.4 HEPES buffer (10 mM).

Fluorescence titration

The interactions of porphyrins **1–3** with G4 DNA were initially investigated by fluorescence spectroscopy (Fig. 3). The telo24 G4 DNA with a hybrid (3 + 1) structure was used. To a solution of each porphyrin (5 μM) in pH 7.4 HEPES buffer (containing 100 mM KCl to induce a hybrid (3 + 1) conformation), G4 was added at varied concentrations. As shown in Fig. 3a, upon addition of G4 DNA, the fluorescence intensity of each porphyrin **1–3** decreased in a dose-dependent manner, indicative of interaction between the porphyrin and G4. Using Stern–Volmer plots, the highest K_q was observed in the case of porphyrin **1** with the shortest linkers (Fig. 3c). Interestingly, the fluorescence quenching was much more significant than that of the previously reported porphyrin **4**.[29]

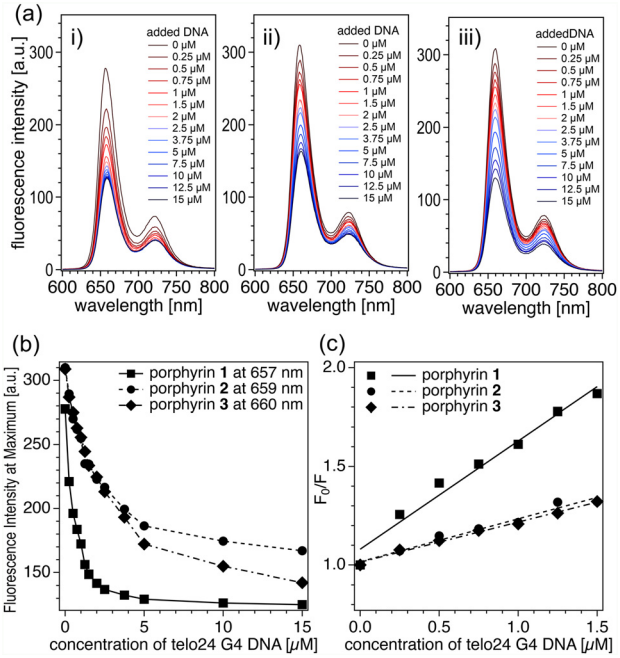

Fig. 3 Fluorescence spectra of porphyrins **1–3** upon addition of telo G4 DNA. (a) Fluorescence spectra of porphyrins **1–3** (5 μM) in the presence of varied concentrations of telo24 G4 DNA (0–15 μM). (b) Dose-dependent decrease of fluorescence intensity of porphyrins **1–3** at emission maxima. (c) Stern–Volmer plot of fluorescence quenching of porphyrins **1–3**. Measurements: in pH 7.4 HEPES (10 mM) containing 1 mM Na_2EDTA and 100 mM KCl; excitation wavelength: 423 nm; slit width: 5 nm.

UV-vis titration

To assess the binding stability of porphyrins **1–3** and G4, UV-vis spectra of porphyrins in the presence of varied concentrations of G4 were recorded. As seen in Fig. 4, similar spectral changes were observed in all porphyrins **1–3** upon the addition of telo24 G4 DNA with a significant intensity decrease of the Soret band. While porphyrins **1** and **2** with shorter linkers showed a slight red shift in the Soret band, porphyrin **3** with longer linkers revealed no significant shift. These changes were similar to those of our previously reported porphyrin **4** and other porphyrins with shorter linkers.[29,30]

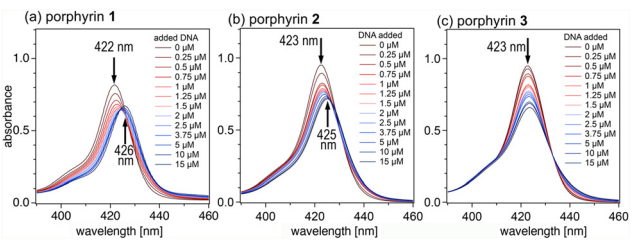

Fig. 4 Interaction of porphyrins **1** (a), **2** (b), and **3** (c) with telomeric G4 DNA shown by UV-vis absorption spectra near the Soret band. Porphyrina (5 μM) and telo24 G4 DNA (0 mM) and telo24 G4 DNA (0–15 μM) in 10 mM HEPES (pH 7.4 with 1 mM Na_2EDTA and 100 mM KCl).

From the UV-vis data, K_d values for complexation of porphyrins to telo24 G4 were determined (Figs. S35 and S38 and Table 1). As a control, hairpin DNA (hpDNA) with a non-G4 structure was employed. As shown in Table 1, significantly lower K_d values were obtained in the case of G4 DNA compared to the control hpDNA for all porphyrins. Among porphyrins **1–3**, porphyrin **1** with shortest linkers showed the highest complexation stability with G4 DNA (K_d = 0.72 μM). However, its complexation stability with G4 was lower than that of our previous porphyrin **4**, although in a similar range. Elongation of the linkers did not contribute to the enhancement of complexation stability.

FRET melting assay for G4-stabilization effects

The above fluorescence and UV-vis measurement assays indicated potential interactions between the porphyrins **1–3** and G4 DNA (Fig. 3 and 4). To further evaluate these interactions, the stabilization effects of the porphyrins on telo24 and Rif1-2 G4 DNAs were studied. Rif1-2 G4 DNA is a recently identified G4-forming sequence and known to bind to replication timing regulatory factor 1 protein (Rif1).[32,33] FRET melting assays were conducted by monitoring FAM emission from dual-labelled telo24 or Rif1-2 G4 DNA in the presence of each of the porphyrins **1–3**. In FRET assay, with an increase in temperature, the G4 structure is disrupted, resulting in a decreased FRET efficiency and a concomitant increase in FAM emission. As a result, the addition of the porphyrins led to a dose-dependent decrease in FAM emission and a corresponding increase in the melting temperature (Tables S39 and S40).

As shown in Fig. 5a, porphyrin **1** showed a stabilization effect on telo24 G4 at concentrations above 0.3 μM, to an extent similar to that shown by TMPyP4, a standard G4 binder. In contrast, porphyrin **3** required higher doses to achieve stabilization, while **2** exhibited the least stabilizing effect. Rif1-2 G4 DNA, a less stable G4 than telo24, was significantly stabilized by porphyrin **1** at 0.3 μM (ΔT_m: 46 °C) and maximally stabilized at ≥0.6 μM concentrations (ΔT_m: >65 °C), an effect similar to that of TMPyP4. Higher concentrations of **2** and **3** were required to stabilize Rif1-2 G4 DNA, mirroring the trend observed with telo24.

Given that some of the known G4 binders are non-specific and interact also with non-G4 DNA, developing selective

Table 1 K_d values of binding of porphyrins **1–4** with telo24 G4 DNA and hairpin (non-G4) DNA obtained from UV-vis titration data

	K_d (SE)[a] [μM]	
Compounds	Telo24 G4 DNA	Hairpin DNA
1	0.72 (0.07)	6.39 (0.56)
2	1.09 (0.18)	11.47 (1.30)
3	2.28 (0.31)	10.75 (1.26)
4	0.34 (0.07)	6.67 (0.87)

[a] Obtained using linear regression on the binding model developed by Wolfe *et al.*[31] using GraphPad Prism 8 software (Fig. S35 and S38 in the SI).

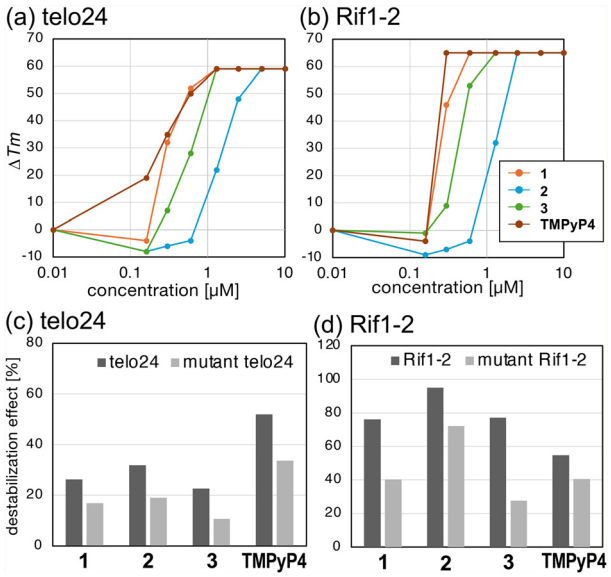

Fig. 5 The stabilization of G4 DNA by **1–3** and G4 specificity analysed by FRET assay. (a and b) The change of T_m values (ΔT_m) of telo24 (a) or Rif1-2 (b) G4 DNA in the presence of **1**, **2**, **3**, or TMPyP4 was plotted (the experiment without the compounds was used as a standard). (c and d) The normalized FAM emission signals of the labelled telo24 (c) or Rif1-2 (d) G4 (0.2 μM) in the presence of compounds **1**, **2**, **3**, or TMPyP4 and competitor (5 μM) wild-type G4 DNA (dark grey) or mutant G4 DNA (light grey).

binders is crucial, especially to target the physiological G4s on the highly transcribed genomes or in rapidly cycling cancer cells. To this end, we performed FRET assays in the presence of two competitors, G4 or non-G4 DNAs, to assess the G4 selectivity of our compounds. All compounds **1–3** demonstrated G4-selectivity for the telo24 DNA during the thermal shift (Fig. S39 and S40a–d). The G4 selectivity rates for **1**, **2**, and **3** were 1.6, 1.7, and 2.1, respectively, comparable to or slightly better than that of TMPyP4 (1.5) (Fig. 5c; Fig, S41a–d and Table S3). Interestingly, the G4 selectivity rates of Rif1-2 for **1** and **3** were significantly higher (1.9 and 2.8, respectively) than those of TMPyP4 (1.4) (Fig. 5d, Fig. S41 and Table S4). These results suggested that our porphyrin compounds may exhibit preferences for specific G4 DNA topologies. CD spectra indicate that Rif1-2 is likely to be parallel-type, whereas telo24 is hybrid and/or anti-parallel type.[33,34] Porphyrins **1–3** may have a preference for the parallel-type, which is often the case for G4 binding proteins *in vivo*. Notably, a prominent feature in the FRET melting curves was observed around 75 °C, particularly in the presence of compound **3** (Fig. S41c and g). While this indicates a potential compound-induced structural transition at elevated temperatures, the G4-selectivity analysis was primarily conducted at $Temp_{\Delta max}$ (see Fig. S42) mostly below 60 °C to ensure quantitative comparisons during the main melting transition. The detailed mechanism behind the high-temperature behavior of compound **3** remains a subject for future investigation.

Photoinduced $^1O_2$ generation by porphyrins 1–3

Photoinduced generation of $^1O_2$ by the porphyrins was investigated by ESR using 4-oxo-TEMP as a spin-trapping agent. In the presence of $^1O_2$, 4-oxo-TEMP forms the adduct 4-oxo-TEMPO, which shows specific signals in the ESR.[35] The obtained ESR signals were quantified to evaluate the amount of $^1O_2$ generated. To be consistent with suitable conditions for PDT, deep-red LED light (maximum at 660 nm) was used. Upon photoirradiation, porphyrins **1–3** generated $^1O_2$ significantly, with a slightly higher amount in the case of porphyrin **2** (Fig. 6a–c). The amount of $^1O_2$ generated by **1–3** was about double that observed for previously reported porphyrin **4**. By taking into account that the absorption intensity of **1–3** at 660 nm was about 2.0–2.7 times higher than that of **4**, the photosensitivity of all porphyrins **1–4** was in a similar range (Fig. S42).

Notably, in the presence of telo24 G4 DNA, photoinduced $^1O_2$ generation by porphyrins **1–3** was highly enhanced (Fig. 6a–d, iii). Upon the addition of 1 equiv. of telo24 G4 DNA to each porphyrin, $^1O_2$ generation was increased 1.3–1.5 times in comparison with the conditions observed when using only the porphyrin. This enhanced $^1O_2$ generation was not significantly observed in the presence of a non-G4 DNA (hpDNA). In UV-vis measurements, no significant intensity increases at 660 nm in the mixtures of porphyrins **1–3** and telo24 were observed. The enhanced $^1O_2$ generation observed here may be related to the microenvironment of porphyrins interacting with G4 DNA to favor $^1O_2$ generation in type II energy transfer reaction steps *e.g.* in photoexcitation or intersystem crossing. Nevertheless, generation of $^1O_2$ by porphyrins **1–3** was significantly higher than that by previously reported **4** and TMPyP4 under 660 nm light, with further enhancement observed in the presence of G4 DNA, indicating their superior properties as PDT-PSs (Table 2).

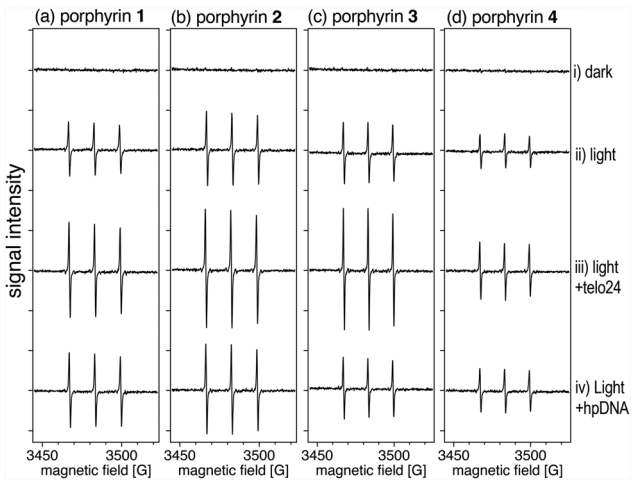

Fig. 6 X band ESR spectra of the $^1O_2$ adduct of 4-oxo-TEMP in solutions of porphyrins **1** (a), **2** (b), **3** (c), and **4** (d) observed under visible light irradiation (maximum at 660 nm) for 10 s. Conditions: porphyrin: 50 μM; 4-oxo-TEMP: 80 mM; KCl: 100 mM; DNA: 50 μM; in 10 mM HEPES buffer (pH 7.4).

Table 2 Effect of G4- and non-G4 DNAs on photoinduced $^1O_2$ generation by porphyrins **1–4**

PSs	Amounts of generated 4-oxo-TEMPO relative to compound **4** [a]		
	PS only control	Telo24 G4 DNA (relative to control)	Hairpin DNA (relative to control)
1	1.98	2.95 (1.49)	2.14 (1.08)
2	2.16	3.54 (1.64)	2.39 (1.11)
3	1.82	2.44 (1.34)	1.83 (1.01)
4	1.00	1.65 (1.65)	1.16 (1.16)

[a] Relative amount of 4-oxo-TEMPO, $^1O_2$ adduct of 4-oxo-TEMP, observed by ESR and calculated from the double integration of the ESR signal (Fig. 6).

Photoinduced DNA cleavage

Photoinduced DNA damage by porphyrins **1–4** was tested on pBR322 supercoiled DNA under visible light irradiation (660 nm LED). pBR322 DNA, which has numerous potential G4 ligand binding sites (20 potential G4 sites predicted by QGRS (quadruplex forming G-rich sequences) Mapper[36]), was used as a substrate DNA, as it is often employed in the assays for oxidative damage of DNA by photosensitizers. The formation of nicked DNA (form II) was quantified by electrophoresis, stained with GelRed®nucleic acid stain and analyzed using ImageJ. Porphyrins **1–3** showed a similar level of photoinduced DNA cleaving activity, with IC_{50} values of 0.11, 0.11, and 0.13 μM, while control porphyrin **4** showed a much reduced effect, with an IC50 value of 0.57 μM (Fig. 7). The result with lowest photocytotoxicity for **4** was in a similar trend to the amount of $^1O_2$ generation by each porphyrin under photoirradiation shown in Fig. 6.

Internalization of porphyrins into the cells

Cellular uptake of PS molecules is an important factor for their function as both G4 binders and PDT-PSs. Taking advantage of the fluorescence intensity of porphyrins **1–3**, cellular uptake of the molecules was assessed by flow cytometry using both a cancer cell line (HeLa) and normal cells (NHDF). The cells were co-incubated with each of porphyrin **1–3** (10 μM) for 24 h. Subsequently, the cells were washed with PBS(−) and treated with trypsin to prepare a cell suspension, which was washed again before being subjected to flow cytometry. A laser excitation of 405 nm and a detection filter of 678–706 nm were used, since all porphyrins **1–3** have almost identical excitation and emission coefficients at these wavelength regions.

Fig. 8 shows flow cytometry histograms for the internalization of each porphyrin. Among the three porphyrins, the cells treated with porphyrin **3** had the highest fluorescence intensity, which was followed by **2** and **1**, indicating that cell internalization efficiency of the porphyrins was **3** > **2** > **1** in both cells. This may be related to the lipophilicity of the porphyrin molecules – porphyrin **3** containing the longest alky linkers with the highest lipophilicity shows higher cellular uptake due to better interaction with the lipid membrane of the cells. The mean fluorescence intensities of porphyrins **1–3** obtained by flow cytometry were higher than that of our previously reported porphyrin **4**, which has shorter linkers with an internalization efficiency of 1.0×10^5 and 3.5×10^5, respectively, for HeLa and NHDF cells (summarized in Table S5). Results showed clearly that elongation of the linkers significantly improved cellular internalization, making these compounds advantageous as G4-targeting drugs and PDT-PSs.

Photocytotoxicity

Encouraged by the results of cellular uptake of porphyrins **1–3** discussed above, photocytotoxicity tests were conducted on both HeLa and NHDF cells. After co-incubation with each porphyrin for 2 h at varied concentrations, cells were washed and irradiated with deep red LED light (max 660 nm) for 15 min and subjected to MTT assay for determining cell viabilities. As a control, previously reported porphyrin **4** was tested under the same conditions. Fig. 9 shows a clear dose-dependent effect of each porphyrin on cell viabilities. IC_{50} values were calculated and are summarized in Table 3. As shown in Fig. 9, all of porphyrins **1–4** showed significant cytotoxicity under visible light irradiation. Slight dark toxicity was observed in porphyrins,

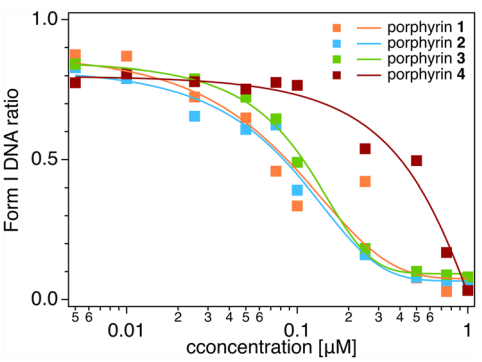

Fig. 7 Concentration-dependent photoinduced DNA cleavage by porphyrins **1**, **2**, **3**, and **4**. The pBR322 supercoiled DNA was used and ratios of form I intact DNA were quantified using ImageJ. Irradiation conditions: light: deep-red LED (maximum at 660 nm); pBR322 DNA: 12.5 μg mL^{-1}; in Tris–HCl-EDTA buffer (pH 8.0); for 10 min.

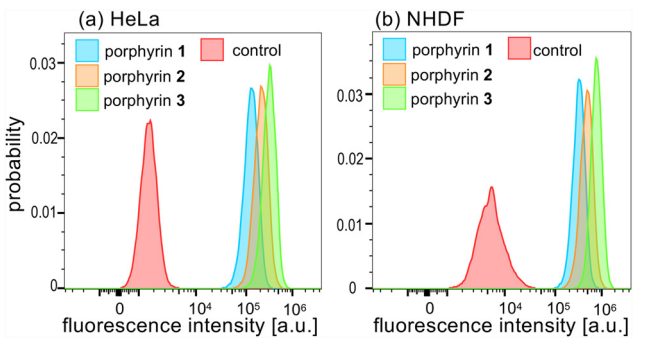

Fig. 8 Flow cytometry histogram for cellular internalization of porphyrins **1**, **2** and **3** in HeLa (a) and NHDF (b). The normalized histograms show the fluorescence observed cells incubated at 10 μM concentration of porphyrin (Ex: 405 nm, Em: 678–706 nm).

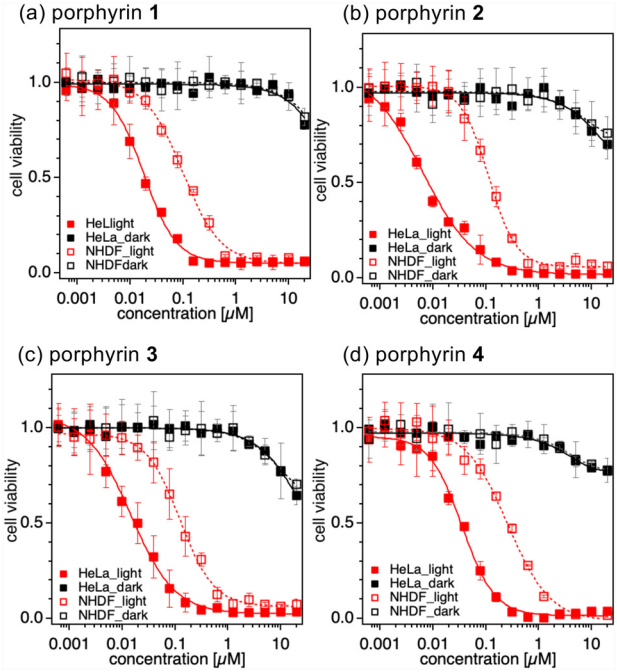

Fig. 9 Photocytotoxicities of porphyrins **1** (a), **2** (b), **3** (c) and **4** (d) under irradiation of a deep red LED (λ_{max} = 660 nm, for 15 min) on HeLa and NHDF cells measured by MTT assay.

Table 3 IC_{50} values for photoinduced cytotoxicity of porphyrins **1–4**

	IC_{50} (SE)[a] [nM]	
compounds	HeLa	NHDF
1	17.9 (1.1)	97.5 (7.3)
2	6.4 (1.3)	113.6 (4.8)
3	14.5 (1.5)	124.5 (7.1)
4	35.4 (3.1)	260.7 (24.8)

[a] Values were obtained from Hill equation fitting of the data points shown in Fig. 9 using Igor Pro 10 software.

especially in those with longer linkers. All compounds showed higher photocytotoxicity toward HeLa cells than toward NHDF cells. Photocytotoxicity of porphyrins **1–3** was much efficient with lower IC_{50} values than that of our previously reported porphyrin **4**, in line with the above-mentioned (1) more efficient generation of $^1O_2$ under deep-red light irradiation (max 660 nm) and (2) better cell internalization effect. Higher phototoxicity toward HeLa cells than toward NHDF cells may be related to the higher abundance of G4 DNA domains in HeLa cells than in normal cells, although this relationship is still unclear. Nevertheless, the results suggest that these porphyrins may be potentially effective in selective damage of cancer cells under visible light irradiation.

Confocal microscopy of permeabilized cells

To identify the interaction of porphyrins **1–3** with cellular components, confocal microscopy measurements were conducted

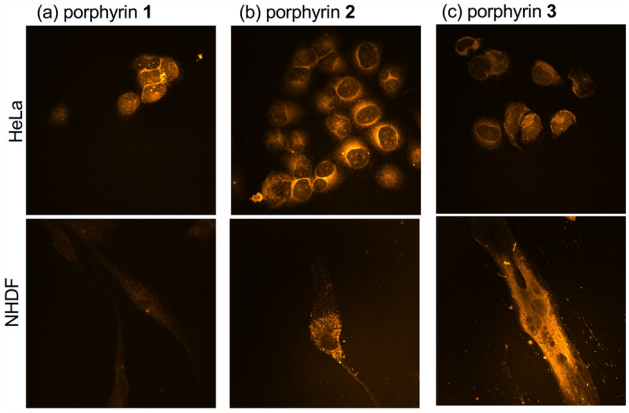

Fig. 10 Confocal microscopy images of HeLa cells and NHDF cells pretreated with 0.5% Triton X-100 for permeabilization and subsequently co-incubated with 5 μM solution of porphyrin **1** (a), **2** (b) or **3** (c) (excitation: 405 nm, filter: ET700/75, image size: 140 × 140 μm).

on HeLa and NHDF cells. Cells were permeabilized using a detergent and fixed prior to the coincubation with porphyrins. Permeabilized cells were treated with each porphyrin (5 μM), washed, and imaged on a confocal microscope with an excitation wavelength of 405 nm and an emission filter of 662.5–737.5 nm to observe the localization of the porphyrins by fluorescence (Fig. 10). All porphyrins **1–3** showed similar localization patterns. In HeLa cells, localization of all three porphyrins was observed as stronger signals in the nucleoli as well as in the cytosolic regions. In NHDF cells, fluorescence signals were spread throughout the cell with punctuated signals in the cytosol shown by emissions, while there was no significant emission in nuclei. The signal observed from the nuclei of the HeLa cells may be related to the interaction of the porphyrins **1–3** with G4 DNA, which is more abundant in cancer cells.

Experimental

Fluorescence spectroscopy

Fluorescence spectroscopy experiments were performed on a Varian Cary Eclipse spectrophotometer (Agilent Technologies, Inc., Santa Clara, California, U.S.). Each solution of **1**, **2**, or **3** (5 μM) was prepared in 10 mM HEPES buffer (pH 7.4, containing 100 mM KCl and 1 mM Na_2EDTA). A solution of single-strand telo24 DNA (500 μM) with the sequence of d(TTAGGGTTAGGGTTAGGGTTAGGG) was prepared in the same buffer and subjected to the pre-annealing process by heating at 90 °C for 10 min and cooling back to room temperature over 3 h. To each porphyrin solution (2 mL) in a quartz cuvette (path length: 1 cm), an aliquot of the DNA solution was added and left to equilibrate for 2 min after mixing to record fluorescence spectra.

UV-vis

UV-vis absorption spectra were recorded on a JASCO V-570 UV/VIS/NIR spectrophotometer (JASCO Co., Tokyo Japan). Each

solution of **1**, **2** or **3** (5 μM) was prepared in 10 mM HEPES buffer (pH 7.4, containing 100 mM KCl and 1 mM Na_2EDTA). A solution of single-strand telo24 DNA (500 μM) with the sequence of d(TTAGGGTTAGGGTTAGGGTTAGGG) was prepared in the same buffer and subjected to the pre-annealing process by heating at 90 °C for 10 min and cooling back to room temperature over 3 hours. To each porphyrin solution (2 mL) in a quartz UV cuvette (path length: 1 cm), an aliquot of the DNA solution was added and left to equilibrate for 2 min after mixing to record UV-vis spectra. The titration was stopped when no change was observed upon the addition of DNA.

FRET melting assay

G4 stabilization by porphyrins was assessed by FRET assay using telo24 and Rif1-2 DNA labeled with 6-carboxyfluorescein (FAM) at the 5′- end and tetramethyl-rhodamine (TAMRA) at the 3′-end (Fasmac Co., Ltd, Kanagawa, Japan). The details are provided in the SI.

Detection of $^1O_2$ using ESR spin trapping reagents

ESR spectra were recorded on a Bruker EMX, Continuous Wave X-Band EPR spectrometer (Bruker BioSpin GmbH). Each measurement was performed on the samples in a Blaubrand® intraMark capillary (50 μL, Brand GMBH, Wertheim, Germany) placed inside a Suprasil® ESR tube (diameter: 4 mm, length: 250 mm, wall thickness: 0.8 mm; SP Wilmad-Lab Glass, NJ, USA). 2,2,6,6-Tetramethylpiperidin-4-one (4-oxo TEMP) was purchased from ABCR (Karlsruhe, Germany) and purified prior to use by sublimation. Nunc MicroWell 96-well round (U) bottom plates were bought from Thermo Scientific (Waltham, MA, USA). Lumidox® II 96-well LED Array (Analytical Sales and Services, Inc., NJ, USA) equipped with a 660 nm max LED was used for light irradiation. DNA oligonucleotides were purchased from Integrated DNA Technologies, Inc. (Coralville, IA, USA). Telo24 G4 DNA with the sequence of d(TTAGGGTTAGGGTTAGGGTTAGGG) was subjected to the pre-annealing process by heating at 90 °C for 10 min and cooling back to room temperature over 3 hours in 10 mM HEPES buffer (pH 7.4, containing 100 mM KCl and 1 mM Na_2EDTA). All measurements were conducted under the same buffer conditions.

DNA photocleavage assay

pBR322 DNA and Gel Loading Dye Purple (6×) were purchased from New England Biolabs (Ipswich, MA, USA). Nunc MicroWell 96 -well round (U) bottom plates were bought from Thermo Scientific (Waltham, MA, USA). Ethylenediaminetetraacetic acid disodium salt dihydrate (EDTA), GelRed® Nucleic Acid Stain 10 000× and agarose were purchased from Sigma-Aldrich (St Louis, MI, USA). Lumidox® II 96-well LED Array (Analytical Sales and Services, Inc., NJ, USA) equipped with a 660 nm max LED was used for light irradiation. Gel Electrophoresis experiments were performed using a Mupid-exU gel electrophoresis system (Mupid Co. Ltd, Tokyo, JAPAN). Imaging of the gels was performed using a ChemiDoc Imaging System (Bio-Rad Laboratories, Inc., CA, USA).

pBR322 DNA was diluted to a stock solution of 25 ng μL^{-1} in Tris-HCl buffer (10 mM, pH 8.0, containing 1 mM EDTA). An aliquot of DNA solution (10 μL) was mixed with 10 μL solution of **1**, **2**, **3** or **4** in Milli-Q water. The mixtures were irradiated with a 96-well illuminator for 10 min using a 660 nm deep red LED light source (330 mW cm^{-2}). Subsequently, Gel Loading Dye Purple 6× (4 μL) was added to each sample prior to loading onto an agarose gel (1% agarose in 0.5× TBE buffer). Electrophoresis experiments were conducted at 100 V for 80 min using 0.5× TBE as the running buffer. The gel was then stained using GelRed® Nucleic Acid Stain 3× (diluted from 10 000× using Milli-Q water) for 1 h. The gels were then imaged using GelRed filter settings. The images were analyzed using ImageJ software.

Cell culture

HeLa and NHDF cells were purchased from ATCC (Manassas, VA, USA). The cells were incubated in DMEM containing 10% FBS supplemented with 2 mM glutamine and 1% penicillin–streptomycin. The pre-cultured semi-confluent cells were dispersed using trypsin and used for the experiments. The following materials were obtained from Thermo Fisher Scientific Inc. (Waltham, Massachusetts, USA): Gibco™ DMEM High Glucose; Gibco™ DMEM high glucose, no glutamine, no phenol red; Gibco™ Fetal Bovine Serum (FBS); Gibco™ Trypsin-EDTA 0.05%, PBS(−) (pH = 7.4, Mg^{2+}, Ca^{2+} free); 200 mM glutamine; Triton X-100; Gibco™ penicillin–streptomycin (10 000 U mL^{-1}).

Flow cytometry

HeLa and NHDF cells were inoculated in a 6-well plate with a density of 3×10^6 cells per well and incubated in DMEM containing 10% FBS and 1% penicillin–streptomycin for 24 h. Subsequently, the cells were incubated in the presence of 10 μM of each porphyrin for an additional 24 h. Cells were trypsinized and centrifuged, and the obtained pellets were washed with PBS(−)three times and resuspended in PBS(−) (500 μL) for measurement. Flow cytometry measurements were performed on a Cytek® Aurora system (Cytek Biosciences, Fermont, CA, USA). Data were analyzed using FlowJo software with the V12 channel (excitation wavelength: 405 nm; emission wavelength: 692 nm (center) with 28 nm width).

Photocytotoxicity assay

3-(4,5-Dimethylthiazol-2-yl)-2,5-diphenyltetrazolium bromide (MTT) and Tween-20 were purchased from Sigma-Aldrich Co. (St Louis, MI, USA). All cells were incubated in Gibco™ DMEM High Glucose containing 10% FBS and 1% penicillin–streptomycin. The 96-well plates were purchased from Techno Plastic Products AG, Trasadingen, Switzerland. A Lumidox® II 96-well LED Array (Analytical Sales and Services, Inc., New Jersey, USA) equipped with deep red LED (660 nm max) was used for photoirradiation. The cell viabilities were evaluated by MTT assay in which OD_{560} was measured using a microplate reader (infinite F200PRO, Group Ltd, Zürich, Switzerland). The means of at

least three independent experiments were reported, and all cell viability results are expressed as means ± SE.

Photocytotoxicity of **1**, **2**, **3**, and **4** was assessed on HeLa and NHDF cells. Preincubated cells were harvested and seeded to a 96-well plate with a density of 1000 cells per well (100 μL) and cultured for 24 h in an incubator at 37 °C under a 5% CO_2 atmosphere. The growth medium in each well was then exchanged with the medium containing each compound, and the cells were incubated under the same conditions for 2 h. Afterwards, cells were washed with PBS(−), and phenol red-free DMEM was added to each well. The cells in 96-well plates were then illuminated for 15 min using 660 nm max deep red light (330 mW cm^{-2}). After the illumination, DMEM was replaced with MTT solution in phenol red-free DMEM (0.5 mg mL^{-1}, 100 μL), and cells were further incubated for 3 h. Subsequently, the medium was removed from each well and replaced with DMSO (100 μL). OD_{560} values were measured using a plate reader. Cell viabilities were calculated from OD560 values relative to negative control where the cells were not treated with any chemicals and positive control where the cells were treated with Tween-20.

Confocal microscopy

All cells were incubated in Gibco™ DMEM High Glucose containing 10% FBS and 1% penicillin–streptomycin. Semi-confluent cells were trypsinized and seeded onto ibidi™ μ-Slide 8 Wells at a density of 10 000 cells per well in 250 μL medium. Cells were incubated in growth medium for 24 h. Subsequently, cells were permeabilized using 0.5% Triton X-100 and fixed using 4% PFA. Afterwards, HeLa and NHDF cells were incubated in the presence of porphyrin solution in PBS(−) for 5 min, washed with PBS(−) and observed under a microscope (excitation: 405 nm laser, emission filter: ET700/75).

Conclusions

In summary, three porphyrin molecules, **1–3**, possessing four imidazolium moieties connected *via* linkers of different lengths were synthesized as potential G4-targeting PSs. The synthesized porphyrins **1–3** showed G4 binding ability with better selectivity than the control porphyrin **4**, as indicated by fluorescence spectroscopy, UV-vis titration, and FRET assay. Among these porphyrins, compound **1** with the shortest linker length displayed the strongest binding to telo24 DNA; however, its effect was weaker than that of the control porphyrin **4**. Upon elongation of linkers, however, selectivity of interaction to G4 DNA over non-G4 DNA was significantly increased in both telo24 and Rif1-2 G4s. All porphyrins **1–3** revealed $^1O_2$ generation under deep-red light irradiation (660 nm), evident from the ESR spin trapping method, at a higher level than control porphyrin **4**. Interestingly, in the presence of telo24 G4 DNA, enhanced $^1O_2$ generation was observed compared with that in its absence. Efficient cellular uptake of the porphyrins was indicated by flow cytometry, and photocytotoxicities were correlated with the efficiency of cellular uptake. As per results, porphyrins **1–3** reported here exhibited superior properties in comparison with the previously reported porphyrin **4** and standard G4 binder TMPyP4 and can be considered as potential core structures for further development of G4-targeted PDT-PSs.

Author contributions

N. Y.-S., H. M., and Y. Y. designed the overall project. C. C. designed detailed structures of the molecules and contributed to their synthesis and structural characterization in collaboration with Y. Y. N. K. and N. Y.-S. performed FRET assay in collaboration with H. M. C. C. performed fluorescence, UV-vis, and CD spectroscopy, ROS generation assay by ESR, DNA cleavage tests, and photocytotoxicity assay in collaboration with Y. Y. C. C. performed fluorescence microscopy analyses in collaboration with S.-S. L. T. X. performed flow cytometry assay in collaboration with C. C. The manuscript was written with contributions from all authors. All authors have given approval to the final version of the manuscript.

Conflicts of interest

There are no conflicts to declare.

Data availability

Supplementary information (SI): experimental data and details regarding the synthesis, ESR, UV-vis, and fluorescence spectroscopy, flow cytometry, DNA photocleavage, photocytotoxicity assays, and fluorescence and confocal microscopy images. See DOI: https://doi.org/10.1039/d6ob00581k.

Acknowledgements

The authors thank Dr Ebert in ETH for his help with the ESR and NMR measurements. The authors thank Prof. Leroux in ETH for his help with the fluorescence measurements. The authors thank Prof. Bode in ETH for his help with CD and UV-vis measurements. ScopeM of ETH, MoBiAS and the NMR service in the D-CHAB at ETH are acknowledged for their help with the measurements.

This research was supported by the SNF Strategic Japanese-Swiss Science and Technology Program (IZLJZ2_183660, Y. Y.), JSPS Joint Research Program implemented in association with SNF (20191508, H. M. and N. Y.-S.), SNF Project Funding (205321_173018, Y. Y.), ETH Research Grants (ETH-21_15-2; ETH-36_20-2, Y. Y.), and JSPS KAKENHI (Grant-in-Aid for Scientific Research [A], 20H00463, H. M.; Grants-in-Aid for Scientific Research on Innovative Areas, 21H00264, 22H04707, H. M.; Fund for the Promotion of Joint International Research (Fostering Joint International Research (B)), 20KK0157, H.M.; Grant-in-Aid for Scientific Research [C], 15K07164, 26K09289, N. Y.-S.).

References

1 N. V. Anantha, M. Azam and R. D. Sheardy, *Biochemistry*, 1998, **37**, 2709–2714.
2 C. L. Grand, H. Han, R. M. Muñoz, S. Weitman, D. D. Von Hoff, L. H. Hurley and D. J. Bearss, *Mol. Cancer Ther.*, 2002, **1**, 565–573.
3 I. M. Dixon, F. Lopez, A. M. Tejera, J.-P. Estève, M. A. Blasco, G. Pratviel and B. Meunier, *J. Am. Chem. Soc.*, 2007, **129**, 1502–1503.
4 U. Chilakamarthi, D. Koteshwar, S. Jinka, N. Vamsi Krishna, K. Sridharan, N. Nagesh and L. Giribabu, *Biochemistry*, 2018, **57**, 6514–6527.
5 M. Gunaratnam, M. d. l. Fuente, S. M. Hampel, A. K. Todd, A. P. Reszka, A. Schätzlein and S. Neidle, *Bioorg. Med. Chem.*, 2011, **19**, 7151–7157.
6 S. Asamitsu, S. Obata, Z. Yu, T. Bando and H. Sugiyama, *Molecules*, 2019, **24**, 429.
7 T.-M. Ou, Y.-J. Lu, C. Zhang, Z.-S. Huang, X.-D. Wang, J.-H. Tan, Y. Chen, D.-L. Ma, K.-Y. Wong, J. C.-O. Tang, A. S.-C. Chan and L.-Q. Gu, *J. Med. Chem.*, 2007, **50**, 1465–1474.
8 P. Podbevšek and J. Plavec, *Nucleic Acids Res.*, 2016, **44**, 917–925.
9 R. Chaudhuri, S. Bhattacharya, J. Dash and S. Bhattacharya, *J. Med. Chem.*, 2021, **64**, 42–70.
10 V. Caprio, B. Guyen, Y. Opoku-Boahen, J. Mann, S. M. Gowan, L. M. Kelland, M. A. Read and S. Neidle, *Bioorg. Med. Chem. Lett.*, 2000, **10**, 2063–2066.
11 I. M. Dixon, F. Lopez, J.-P. Estève, A. M. Tejera, M. A. Blasco, G. Pratviel and B. Meunier, *ChemBioChem*, 2005, **6**, 123–132.
12 L. Finlayson, I. R. M. Barnard, L. McMillan, S. H. Ibbotson, C. T. A. Brown, E. Eadie and K. Wood, *Photochem. Photobiol.*, 2022, **98**, 974–981.
13 P. Agostinis, K. Berg, K. A. Cengel, T. H. Foster, A. W. Girotti, S. O. Gollnick, S. M. Hahn, M. R. Hamblin, A. Juzeniene, D. Kessel, M. Korbelik, J. Moan, P. Mroz, D. Nowis, J. Piette, B. C. Wilson and J. Golab, *Ca-Cancer J. Clin.*, 2011, **61**, 250–281.
14 H. Abrahamse and M. R. Hamblin, *Biochem. J.*, 2016, **473**, 347–364.
15 M. Deiana, J. M. Andrés Castán, P. Josse, A. Kahsay, D. P. Sánchez, K. Morice, N. Gillet, R. Ravindranath, A. K. Patel, P. Sengupta, I. Obi, E. Rodriguez-Marquez, L. Khrouz, E. Dumont, L. Abad Galán, M. Allain, B. Walker, H. S. Ahn, O. Maury, P. Blanchard, T. Le Bahers, D. Öhlund, J. von Hofsten, C. Monnereau, C. Cabanetos and N. Sabouri, *Nucleic Acids Res.*, 2023, **51**, 6264–6285.
16 X. Zhang and M.-H. Hu, *Sens. Actuators, B*, 2025, **425**, 136952.
17 D. Lin, W. Long, B. Zheng, J. Zhu, H. Yang, G. Song, D. Yan, Y. Liu, L. Wang, D. Wang and B. Z. Tang, *Sens. Actuators, B*, 2026, **448**, 139052.
18 X.-D. Wang, J.-H. Lin and M.-H. Hu, *J. Biol. Chem.*, 2026, **302**, 111181.
19 Q. Wu, W.-W. Hong, J.-H. Shi, R.-S. Deng, W.-Q. Chen, C.-L. Yuan and W.-J. Mei, *Aggregate*, 2026, **7**, e70239.
20 Y. Dong and M. H. Hu, *Eur. J. Med. Chem.*, 2026, **302**, 118292.
21 X. D. Wang, Y. S. Liu, Z. L. Liang and M. H. Hu, *Eur. J. Med. Chem.*, 2025, **289**, 117489.
22 X. Zhang, J. X. Wang and M. H. Hu, *ACS Pharmacol. Transl.*, 2024, **7**, 2174–2184.
23 G. Biffi, D. Tannahill, J. McCafferty and S. Balasubramanian, *Nat. Chem.*, 2013, **5**, 182–186.
24 R. Hänsel-Hertsch, D. Beraldi, S. V. Lensing, G. Marsico, K. Zyner, A. Parry, M. Di Antonio, J. Pike, H. Kimura, M. Narita, D. Tannahill and S. Balasubramanian, *Nat. Genet.*, 2016, **48**, 1267–1272.
25 R. Hänsel-Hertsch, M. Di Antonio and S. Balasubramanian, *Nat. Rev. Mol. Cell Biol.*, 2017, **18**, 279–284.
26 J. An, M. Yin, J. Yin, S. Wu, C. P. Selby, Y. Yang, A. Sancar, G.-L. Xu, M. Qian and J. Hu, *Nucleic Acids Res.*, 2021, **49**, 12252–12267.
27 J. Osterloh and M. G. H. Vicente, *J. Porphyrins Phthalocyanines*, 2002, **06**, 305–324.
28 S. Cogoi and L. E. Xodo, *Chem. Commun.*, 2010, **46**, 7364–7366.
29 Ç. Çelik, N. Kakusho, T. Xu, S. Sik Lee, N. Yoshizawa-Sugata, H. Masai and Y. Yamakoshi, *RSC Med. Chem.*, 2026, **17**, 225–235.
30 C. Wei, L. Wang, G. Jia, J. Zhou, G. Han and C. Li, *Biophys. Chem.*, 2009, **143**, 79–84.
31 A. Wolfe, G. H. Shimer and T. Meehan, *Biochemistry*, 1987, **26**, 6392–6396.
32 Y. Kanoh, S. Matsumoto, R. Fukatsu, N. Kakusho, N. Kono, C. Renard-Guillet, K. Masuda, K. Iida, K. Nagasawa, K. Shirahige and H. Masai, *Nat. Struct. Mol. Biol.*, 2015, **22**, 889–897.
33 H. Masai, N. Kakusho, R. Fukatsu, Y. Ma, K. Iida, Y. Kanoh and K. Nagasawa, *J. Biol. Chem.*, 2018, **293**, 17033–17049.
34 A. Ambrus, D. Chen, J. Dai, T. Bialis, R. A. Jones and D. Yang, *Nucleic Acids Res.*, 2006, **34**, 2723–2735.
35 Y. Lion, M. Delmelle and A. Van De Vorst, *Nature*, 1976, **263**, 442–443.
36 O. Kikin, L. D'Antonio and P. S. Bagga, *Nucleic Acids Res.*, 2006, **34**, W676–W682.